

Semidefinite programming for self-consistent quantum measurement tomography

Marco Cattaneo,^{1,2,3,*} Elsi-Mari Borrelli,¹ Guillermo García-Pérez,¹
Matteo A. C. Rossi,^{1,4} Zoltán Zimborás,^{1,5} and Daniel Cavalcanti¹

¹*Algorithmiq Ltd, Kanavakatu 3C 00160 Helsinki, Finland*

²*QTF Centre of Excellence, Department of Physics,*

University of Helsinki, P.O. Box 43, FI-00014 Helsinki, Finland

³*Instituto de Física Interdisciplinar y Sistemas Complejos (IFISC, UIB-CSIC),
Campus Universitat de les Illes Balears E-07122, Palma de Mallorca, Spain*

⁴*QTF Centre of Excellence, Department of Applied Physics,
School of Science, Aalto University, FI-00076 Aalto, Finland*

⁵*Wigner Research Centre for Physics, H-1525 Budapest P.O. Box 49, Hungary*

(Dated: December 21, 2022)

We propose an estimation method for quantum measurement tomography (QMT) based on a semidefinite program (SDP), and discuss how it may be employed to detect experimental errors, such as shot noise and/or faulty preparation of the input states on near-term quantum computers. Moreover, if the positive operator-valued measure (POVM) we aim to characterize is informationally complete, we put forward a method for self-consistent tomography, i.e., for recovering a set of input states and POVM effects that is consistent with the experimental outcomes and does not assume any a priori knowledge about the input states of the tomography. Contrary to many methods that have been discussed in the literature, our method does not rely on additional assumptions such as low noise or the existence of a reliable subset of input states.

I. INTRODUCTION

Quantum measurement tomography (QMT) may be defined as the complete characterization of a measurement performed on a quantum system by reconstructing the corresponding *positive operator-valued measure* (POVM) [1]. This technique is of crucial importance, for instance, for monitoring the properties of near-term quantum computers and for recovering information on the quantum state at a given step of a quantum algorithm.

For example, in algorithms such as the variational quantum eigensolver (VQE), one needs to evaluate expectation values of operators on a trial state. The expectation value is obtained through repeated measurements of the trial state. Since the physical measurement process is generally faulty and the realised measurement operator may differ significantly from the idealised one, one typically obtains biased estimates, jeopardizing the convergence of the algorithm.

Generally, read-out noise mitigation strategies aim at correcting the empirical distribution of outcomes by modelling the measurement error. These approaches usually considers only projective measurements and stochastic errors as specific error models [2–9]. In order to use advanced measurement strategies [10–14], and address realistic noise models, more general methods should be considered.

While, ideally, measurement tomography returns the exact POVM associated with the measurement apparatus, in real experiments we usually have to deal with shot

noise and imperfect preparation of the tomographic input states. This is why a fitting method, such as maximum likelihood estimation [15] (which we review in Sec. III), are typically employed to obtain a set of physical POVM effects from the outcomes of the tomographic experiment.

Self-consistent tomography consists in a tomographic experiment where no a priori knowledge on the list of input states, on the measurement effects and/or on the experimental gates is assumed, so that the so-called *SPAM* (preparation and measurement) errors cannot jeopardize the tomographic results. Several studies on self-consistent tomography have been presented during the past ten years [16–27].

In this paper, we put forward a fitting method for QMT based on a semidefinite program (SDP); a class of convex optimisation problems which can be solved with very efficient numerical methods [28, 29]. The paper is structured as follows. In II we briefly introduce the concept of quantum measurement tomography. Our SDP based method is described in Sec. IV and in Sec. V we show, how they can be used to diagnose errors in QMT. Finally, in Sec. VI, we discuss a a see-saw optimisation based *self-consistent* QMT for informationally complete POVMs, that does not rely on additional assumptions.

II. QUANTUM MEASUREMENT TOMOGRAPHY

Let us now formalize the concept of quantum measurement tomography, which aims to characterize the measurement we may perform on a quantum system as a positive operator-valued measure (POVM) [1]. We point out that the term “quantum detector tomography” is also commonly employed in the literature [2, 3, 30–34]. In this

* marco.cattaneo@algorithmiq.fi

work, we prefer “measurement tomography” because we are discussing the characterization of a generic POVM that may arise in a plethora of different physical situations, which may not involve proper detectors.

Let us suppose that the measurement we are interested in has m different outcomes. According to quantum mechanics, each outcome can be associated with an operator Π_k (also called an *effect*), and all the effects satisfy the following properties:

$$\Pi_k \geq 0 \quad \forall k, \quad \sum_{k=1}^m \Pi_k = \mathbb{I}. \quad (1)$$

The set of effects $\{\Pi_k\}_{k=1}^m$ fully characterises the measurement, since the outcome probabilities for any quantum state ρ can be computed according to the Born rule $p_k = \text{Tr}(\rho\Pi_k)$. Thus, the goal of QMT is to, given an uncharacterised measurement apparatus, provide a description of its measurement effects $\{\Pi_k\}_{k=1}^m$.

The standard way to perform QMT is to prepare a tomographically complete set of states $\{\rho_j\}_{j=1}^N$ [15, 35, 36] and measure them with the uncharacterised measurement. To be tomographically complete, the set must contain at least d^2 linearly independent states. If this is the case, by knowing the outcome probabilities $p_{jk} = \text{Tr}[\rho_j\Pi_k]$ we can obtain each effect Π_k by linear inversion.

However, in real experiments we never know the probabilities p_{jk} exactly. This is because we can only obtain a finite number n_S of measurement shots, which allows us to obtain the frequencies

$$f_{jk} = \frac{C_{jk} * N}{n_S}, \quad (2)$$

where C_{jk} is the number of times we have obtained the k th outcome when measuring the j th state and n_S/N is the number of times we prepare each state. These frequencies are just an approximation of the true probabilities as $\lim_{n_S \rightarrow \infty} f_{jk} = p_{jk}$. As a consequence, if we apply standard linear inversion starting from $\{f_{jk}\}$, we may obtain non-physical effects $\{\Pi_k\}_{k=1}^m$ (i.e., they may not all be positive) due to finite statistics [15]. A commonly applied strategy for constructing a valid POVM from finite statistics is based on maximum likelihood estimation described in the following section.

III. MAXIMUM LIKELIHOOD FOR MEASUREMENT TOMOGRAPHY

Since standard linear inversion may not yield a physical set of effects, we need to have ways of providing sensible (i.e. physical) estimates of $\{\Pi_k\}_{k=1}^m$ given $\{f_{jk}\}$ and $\{\rho_j\}_{j=1}^N$. A widely used method is given by maximum-likelihood estimation [15]. The idea of this method is to maximize the likelihood functional

$$\mathcal{L}[\{\Pi_k\}_{k=1}^m] = \prod_{j=1}^N \prod_{k=1}^m (\text{Tr}[\rho_j\Pi_k])^{f_{jk}}, \quad (3)$$

in the subspace of physical effects, i.e.

$$\begin{aligned} \max_{\{\Pi_k\}} \quad & \prod_{j=1}^N \prod_{k=1}^m (\text{Tr}[\rho_j\Pi_k])^{f_{jk}} \\ \text{s.t.} \quad & \Pi_k \geq 0 \quad \forall k \\ & \sum_{k=1}^m \Pi_k = \mathbb{I}. \end{aligned} \quad (4)$$

where the input data for the estimation are the set of states $\{\rho_j\}_{j=1}^N$ and the experimental frequencies f_{jk} . We notice that this maximisation is equivalent to minimising the negative of the logarithm of the likelihood functional

$$-\log \mathcal{L}[\{\Pi_k\}_{k=1}^m] = -\sum_{j=1}^N \sum_{k=1}^m f_{jk} \log(\text{Tr}[\rho_j\Pi_k]). \quad (5)$$

This is a convex optimization problem, which is more suited to be solved numerically [37, 38].

Moreover, in the case of Gaussian shot noise, the maximum likelihood (3) becomes equivalent to a least-square approximation [39]:

$$\begin{aligned} \min_{\{\Pi_k\}} \quad & \sum_{jk} [f_{jk} - \text{Tr}(\rho_j\Pi_k)]^2 \\ \text{s.t.} \quad & \Pi_k \geq 0 \quad \forall k \\ & \sum_{k=1}^m \Pi_k = \mathbb{I}. \end{aligned} \quad (6)$$

This kind of least-square problem for measurement tomography has been recently analysed in some works that put forward a two-stage estimation of the POVM effects [40–42].

IV. SEMIDEFINITE PROGRAMS FOR MEASUREMENT TOMOGRAPHY

In this section we propose an alternative to the maximum likelihood estimation and solve QMT through the following optimisation problem:

$$\begin{aligned} \min_{\{\Pi_k\}} \quad & \|\mathbf{f} - \mathbf{q}\| \\ \text{s.t.} \quad & \Pi_k \geq 0 \quad \forall k \\ & \sum_{k=1}^m \Pi_k = \mathbb{I}, \end{aligned} \quad (7)$$

where \mathbf{f} is the vector of frequencies f_{jk} and \mathbf{q} is a vector with components $\text{Tr}(\rho_j\Pi_k)$, while $\|\mathbf{x}\|$ is some norm of the vector \mathbf{x} . This family of optimisation problems looks for the closest quantum distribution to the measured frequencies, where the notion of closeness is given by the specific norm. For instance, (6) is equivalent to minimising using the (square of) the Euclidian norm $\|\mathbf{x}\|_2 = \sqrt{\sum_i x_i^2}$.

In this paper, we will focus on two particular choices for the norm: $\|\mathbf{x}\|_1 = \sum_i |x_i|$ and $\|\mathbf{x}\|_\infty = \max_i |x_i|$. The

main reason for these choices is that, as we will show in what follows, they allow us to write the optimisation problems (7) as semidefinite programs (SDPs) for which efficient algorithms exist [28].

1. Infinite norm, a.k.a. Single-delta SDP

Let us first choose the infinite norm, for which (7) becomes

$$\begin{aligned} \min_{\{\Pi_k\}} \quad & \max_{jk} |f_{jk} - \text{Tr}(\rho_j \Pi_k)| \\ \text{s.t.} \quad & \Pi_k \geq 0 \quad \forall k \\ & \sum_{k=1}^m \Pi_k = \mathbb{I}. \end{aligned} \quad (8)$$

At first sight this seems to be a min-max problem over a non-linear objective function (because of the norm), but one can easily transform it into an SDP by noticing that the biggest absolute value of an entry of a vector \mathbf{x} is the minimum value of $\delta \geq 0$ such that $-\delta \mathbf{1} \leq \mathbf{x} \leq \delta \mathbf{1}$, where $\mathbf{1} = (1, \dots, 1)^T$. Thus, the optimisation problem (8) can be rewritten as

$$\begin{aligned} \min_{\{\Pi_k\}} \quad & \delta \\ \text{s.t.} \quad & \delta \geq 0 \\ & f_{jk} - \delta \leq \text{Tr}(\rho_j \Pi_k) \leq f_{jk} + \delta \quad \forall j, k \\ & \Pi_k \geq 0 \quad \forall k \\ & \sum_{k=1}^m \Pi_k = \mathbb{I}. \end{aligned} \quad (9)$$

Now the problem involves just a minimisation of a single parameter δ . Once an instance of this SDP is solved, we have both the solution δ^* and the effects $\{\Pi_k^*\}$ that satisfy all the constraints (i.e. define a valid POVM). Moreover, the SDP has a very neat interpretation: δ can be seen as a perturbation to the frequencies f_{jk} , so that the solution of the SDP δ^* quantifies the minimum amount of perturbation we need to add to the frequencies so that they have a quantum realisation. For instance, if $\delta^* = 0$, no perturbation is needed and we can find effects $\{\Pi_k\}$ such that $\text{Tr}(\rho_j \Pi_k) = f_{jk} \quad \forall j, k$.

2. 1-norm, a.k.a. Many-deltas SDP

The other norm that we analyse is the 1-norm, for which (7) becomes

$$\begin{aligned} \min_{\{\Pi_k\}} \quad & \sum_{jk} |f_{jk} - \text{Tr}(\rho_j \Pi_k)| \\ \text{s.t.} \quad & \Pi_k \geq 0 \quad \forall k \\ & \sum_{k=1}^m \Pi_k = \mathbb{I}. \end{aligned} \quad (10)$$

We can use the same reasoning as before and rewrite this optimisation problem as

$$\begin{aligned} \min_{\{\Pi_k\}} \quad & \sum_{jk} \delta_{jk} \\ \text{s.t.} \quad & \delta_{jk} \geq 0 \quad \forall j, k \\ & f_{jk} - \delta_{jk} \leq \text{Tr}(\rho_j \Pi_k) \leq f_{jk} + \delta_{jk} \quad \forall j, k \\ & \Pi_k \geq 0 \quad \forall k \\ & \sum_{k=1}^m \Pi_k = \mathbb{I}. \end{aligned} \quad (11)$$

Notice that now we have added one perturbation δ_{jk} to each f_{jk} , which implies having more variables than the SDP (9). At the same time, now we can have more fine-tuned information about which frequencies need to be perturbed more to have a physical description. As we will show later, we can explore this for detecting mismatches in the experiment.

In the next chapters we will numerically investigate the performance of these SDPs. Our numerics were run using the MOSEK solver [43] at CVXPY [44, 45].

V. QUANTIFYING THE IMPACT OF NOISE IN QMT THROUGH SEMIDEFINITE PROGRAMMING

Different types of noise are always present in any quantum experiment, and influence the QMT process. For instance, shot noise, i.e., the noise coming from the fact that we can only perform a finite number of experimental shots, is responsible for the mismatch between the ideal outcome probabilities and the experimental frequencies. Another possible source of noise is due to the fact that QMT assumes that we perfectly know the set of input states $\{\rho_j\}_{j=1}^N$. This is a very strong assumption that is almost never valid in current quantum experiments. In this section, we will see how these types of noise impact the performance of QMT and how the SDPs provided above can be used to diagnose them.

A. Shot noise

To detect the effects of shot noise on measurement statistics we will employ exclusively the single-delta SDP, as shot noise is uniform over all the input states and effects of QMT. The solution δ^* of Eq. (9) is a measure of the mismatch between the ideal probabilities associated with the set of output effects and the experimental frequencies. Therefore, intuitively it should decrease by increasing the number of shots. We quantitatively investigate this behaviour by performing 100 different numerical simulations of QMT on a single-qubit *SIC-POVM* (Symmetric informationally complete POVM) [46] with 4 random linearly independent input states and for different number of shots n_S . More specifically, the effects

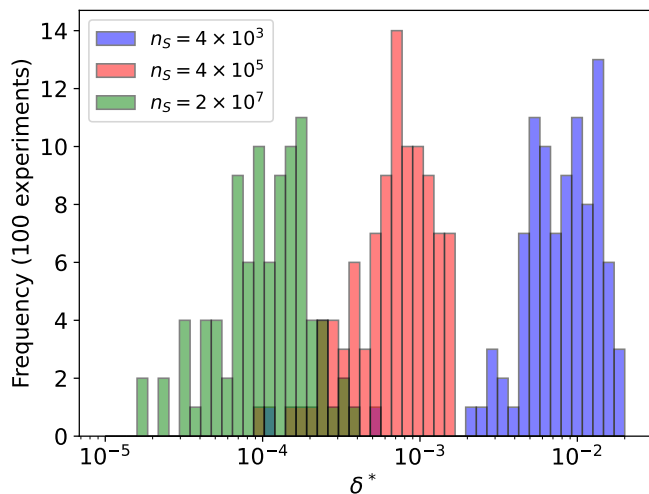


FIG. 1. Distribution of the values of δ^* returned by the single-delta SDP according to Eq. (9) for QMT on the SIC-POVM with 4 random input states (100 numerical experiments), for different total numbers of shots n_S . In the plot, we are not showing a few outliers around 10^{-8} due to favourable frequency samplings that are close to the ideal case ($f_{jk} \approx p_{jk}$).

of the SIC-POVM can be written in the Bloch representation as [46]:

$$\Pi_k^{(\text{SIC})} = \frac{1}{4}\mathbb{I} + \frac{1}{4}\mathbf{n}_k \cdot \boldsymbol{\sigma}, \quad (12)$$

where $\boldsymbol{\sigma} = (\sigma_x, \sigma_y, \sigma_z)^T$ and \mathbf{n}_k are unit vectors given by:

$$\begin{aligned} \mathbf{n}_1 &= (0, 0, 1)^T, \\ \mathbf{n}_2 &= \left(\frac{2\sqrt{2}}{3}, 0, -\frac{1}{3} \right)^T, \\ \mathbf{n}_3 &= \left(-\frac{\sqrt{2}}{3}, \sqrt{\frac{2}{3}}, -\frac{1}{3} \right)^T, \\ \mathbf{n}_4 &= \left(-\frac{\sqrt{2}}{3}, -\sqrt{\frac{2}{3}}, -\frac{1}{3} \right)^T. \end{aligned} \quad (13)$$

Our numerical tests of 100 experiments consisted of the following steps: i) We first generated a set of 4 random linearly independent input states (density matrices) $\{\rho_j\}_{j=1}^4$ through a suitable function available in Qutip [47]. ii) We then simulated n_S total measurement runs of the SIC-POVM on the this set of input states by sampling the probability distribution given by $p_{jk} = \text{Tr}[\rho_j \Pi_k^{(\text{SIC})}]$ (for each input state we therefore use $n_S/4$ shots), which produced the frequencies f_{jk} . iii) We used these frequencies and the set $\{\rho_j\}_{j=1}^4$ as inputs to the single-delta SDP (9) and obtained the solution δ^* and the corresponding set of effects $\{\Pi_k^*\}$ achieving it.

The results of our simulation are shown in Fig. 1, where we plot a histogram distribution over the 100 numerical

experiments of the final values δ^* for different number of shots n_S . As expected δ^* is statistically smaller if n_S is higher. This is consistent with the fact that QMT is more accurate when more shots are performed, and it returns the exact effects of the POVM we aim to characterize in the limit $n_S \rightarrow \infty$.

In addition, we have repeated the same tomographic experiments with different numbers of input states N . If $N = 4$, then we have a complete set of states for QMT of the SIC-POVM. If $N > 4$, we say that we have an *overcomplete* set of input states. We have once again run 100 numerical experiments of QMT with complete and overcomplete set of input states. We plot in Fig. 2 (left) the mean value of δ over the 100 experiments as a function of the total number of shots n_S and for different numbers of input states N . For finite numbers of shots there is trade-off between the number of input states, which add information on the POVM effects, and the number of shots that is split into the different inputs. In Fig. 2 (left) we observe that δ^* is larger if N is larger, so, in this case, this trade-off is privileging more shots for less inputs.

Furthermore, to compare the value of δ with the actual accuracy of QMT, we have computed the average trace distance [1] between the ideal effects of the SIC-POVM in Eq. (12) and the output effects returned by the SDP. The results are displayed in Fig. 2 (right). As expected, the trace distance is smaller for a larger number of shots. Moreover, we observe that, in this case, the trade-off between number of input states and number of shots per input states is privileging the scenarios with $N = 7$ and $N = 4$.

Finally, we observe that both δ^* and the trace distance respect the scaling we expect from shot noise, which is proportional to $1/\sqrt{n_S}$.

B. Faulty preparation of input states

Another crucial source of errors in QMT consists in mismatches between the assumed input states, and the actually prepared ones. If the frequencies observed came from measurements on different states than the ones assumed, the optimisation method (being it MLE, SDP, or any other) will be driven to an erroneous POVM, even in the infinite statistics situation. In this section, we show how the solutions δ^* of Eq. (9) and $\delta_{j,k}^*$ of Eq. (11) can be employed to detect noise in the preparation of the input states for QMT. In particular, we will analyze two separate types of noise, namely *incoherent noise* and *coherent noise*.

For both coherent and incoherent noise, we will study the effects of noisy maps that vary among the input states. This is because, if we apply the same map ϕ to all input states, we run into a *gauge*-freedom problem in the measurement tomography. That is, if the real set of effects is $\{\Pi_k\}_{k=1}^m$, QMT will return (up to shot noise) the set $\{\phi^\dagger[\Pi_k]\}_{k=1}^m$, because $\text{Tr}[\phi[\rho_j]\Pi_k] = \text{Tr}[\rho_j\phi^\dagger[\Pi_k]]$.

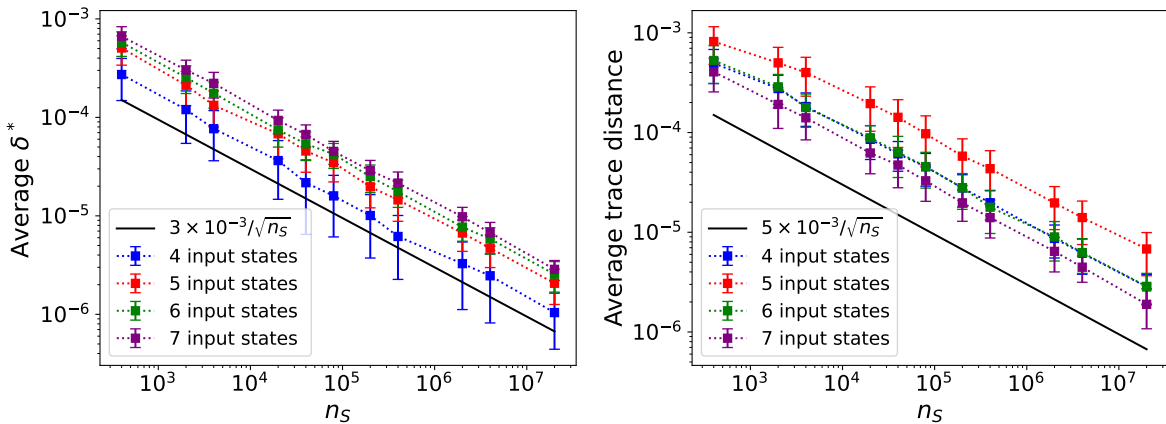


FIG. 2. Left: average δ^* as a function of the total number of shots n_S returned by the single-delta SDP according to Eq. (9) over 100 numerical experiments on QMT for the SIC-POVM and for different numbers of random input states. Right: for the same experimental conditions, average trace distance between the estimated effects of the single-delta SDP and the corresponding effects of the SIC-POVM. The trace distance is averaged over both different experiments and different effects. The error bars in both plots are given by the standard deviations of the samples over the different experiments. The shot-noise scaling proportional to $1/\sqrt{n_S}$ is also shown in both plots.

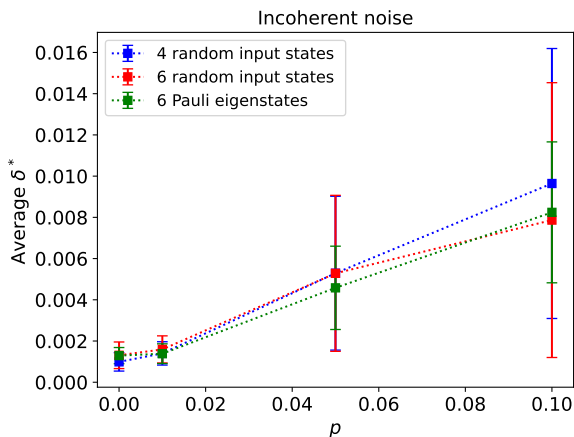


FIG. 3. Average δ^* as a function of incoherent noise strength p on the input states, returned by the single-delta SDP over 100 numerical experiments on QMT for the SIC-POVM and for different sets of input states. The error bars are given by the standard deviations of the samples over the different experiments. We are using a total number of shots $n_S = 6 \times 10^5$.

As a consequence, we will not obtain higher values of δ^* . This gauge loophole is avoided if we apply a different map on each input state. Moreover, varying the noise on the input states is also a more physical description of real errors on near-term quantum computers, as different input states are prepared through different gates, and therefore are subject to different noise sources and magnitudes.

1. Incoherent noise

We say that a noise channel is “incoherent” if it is reducing the purity of the quantum state of the system. One of the most common examples of incoherent noise is the *depolarizing channel* [1], defined as

$$\phi_p^{\text{dep}}[\rho] = (1-p)\rho + \frac{p}{2}\mathbb{I}, \quad (14)$$

where $p = [0, 1]$ can be considered as the noise strength. Another incoherent noise channel is the *amplitude damping channel* [1]:

$$\phi_p^{\text{amp}}[\rho] = K_{0,p}\rho K_{0,p}^\dagger + K_{1,p}\rho K_{1,p}^\dagger, \quad (15)$$

with

$$K_{0,p} = \begin{pmatrix} 1 & 0 \\ 0 & \sqrt{1-p} \end{pmatrix}, \quad K_{1,p} = \begin{pmatrix} 0 & \sqrt{p} \\ 0 & 0 \end{pmatrix}. \quad (16)$$

Finally, a third example of incoherent noise is given by the *phase damping channel* [1]:

$$\phi_p^{\text{ph}}[\rho] = E_{0,p}\rho E_{0,p}^\dagger + E_{1,p}\rho E_{1,p}^\dagger, \quad (17)$$

with

$$E_{0,p} = \begin{pmatrix} 1 & 0 \\ 0 & \sqrt{1-p} \end{pmatrix}, \quad E_{1,p} = \begin{pmatrix} 0 & 0 \\ 0 & \sqrt{p} \end{pmatrix}. \quad (18)$$

Let us now construct a quantum map that depends on the value of a 3-outcome random variable $X = 0, 1, 2$, where the three outcomes have equal probability. The quantum map can be written as:

$$\phi_p^{(X)} = \begin{cases} \phi_p^{\text{dep}} & \text{if } X = 0, \\ \phi_p^{\text{amp}} & \text{if } X = 1, \\ \phi_p^{\text{ph}} & \text{if } X = 2. \end{cases} \quad (19)$$

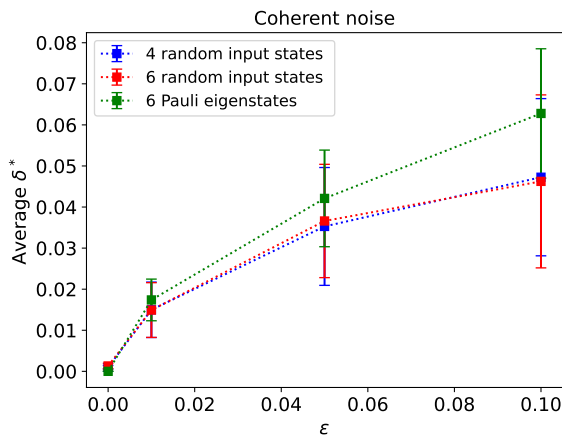


FIG. 4. Average δ^* as a function of coherent noise magnitude ϵ on the input states, returned by the single-delta SDP over 100 numerical experiments on QMT for the SIC-POVM and for different sets of input states. The error bars are given by the standard deviations of the samples over the different experiments. We are using a total number of shots $n_S = 6 \times 10^5$.

We now simulate a set of N input states by drawing a different value of X for each input state and then applying $\phi_p^{(X)}$ thereof. Eventually, we prepare the set $\{\phi_p^{(X)}[\rho_j]\}_{j=1}^N$, where X can vary among the input states.

Using the above prescription, we have performed 100 numerical QMT experiments to characterize the SIC-POVM introduced in Sec. V A, with different values of incoherent noise p on the input states. The numerical experiments have been performed following the same lines as for shot noise. The results for δ^* according to the single-delta SDP are depicted in Fig. 3 for the same sets of 4 and 6 random input states we used in the case of incoherent noise, and for a specific set of pure input states (before noise) given by the eigenvectors of the Pauli matrices. We observe that δ^* is capturing the incoherent noise on the input states for all the sets.

2. Coherent noise

Coherent noise can be defined as the application of (undesired) unitary rotations to the input states of QMT. A generic 1-qubit rotation can be characterized by three angles, namely ϕ , φ , and ψ , as follows:

$$U(\phi, \varphi, \psi) = \begin{pmatrix} e^{i\psi} \cos \phi & -e^{-i\varphi} \sin \phi \\ e^{i\varphi} \sin \phi & e^{-i\psi} \cos \phi \end{pmatrix}. \quad (20)$$

We now focus on numerical experiments on QMT of the SIC-POVM, as discussed in the previous sections, but with only coherent noise (no incoherent noise, i.e., $p = 0$ in Eq. (19)). We generate a uniformly random rotation by sampling uniformly ψ and φ from $[0, 2\pi]$ and a quantity ζ uniformly from $[0, 1]$; then, we compute

$\phi = \arcsin \sqrt{\zeta}$ [48]. We perform sets of 100 numerical experiments by varying the set of input states and the coherent noise magnitude $\epsilon < 1$, which is used to scale ψ and ϕ in Eq. (20) (that is, we sample, e.g., ψ as discussed above and then we multiply it by ϵ , and the same for ϕ). In this way, we construct a random unitary rotation that is close to the identity (the parameter φ does not need to be of the order of ϵ to obtain such a small perturbation). We sample a different unitary rotation for each input state, and then we prepare a set of noisy input states as $\{U(\phi, \varphi, \psi)[\rho_j]\}_{j=1}^N$, where the parameters of U are sampled and scaled by ϵ for each j .

We plot in Fig. 4 the average value of δ^* returned by the single-delta SDP as a function of the coherent noise magnitude ϵ^* . We immediately realize that this quantity is able to capture the presence of coherent noise in the input states for any number N thereof. Moreover, even a small amount of coherent error in the state preparation is inducing a relevant δ^* (typically, for the same magnitude of p and ϵ , one order of magnitude higher than for incoherent noise), therefore we can conclude that δ^* will be able to detect noise in the input states in most of the experimental realizations of QMT on near-term quantum computers.

3. Predominant noise on a subset of input states

So far, we have explored the effects of noise acting randomly on each input state with the same magnitude, treating all of the states on the same footing. This is not always the case in real experimental conditions. For instance, in many of the current devices the initial state of the qubit is prepared in the ground state, and this initialization may be assumed to be more reliable than, for instance, the preparation of an entangled multi-qubit state that requires several CNOT gates. In these situations, the many-deltas SDP can be employed to detect unbalanced noise among the input states.

We have performed two sets of 100 numerical experiments of QMT with the SIC-POVM through the many-deltas SDP and adding noise on some input states only. Specifically, we have chosen as initial input states the set of 6 eigenstates of the Pauli matrices, where we denote $|\pm z\rangle$ as the eigenstate of σ_z with eigenvalue ± 1 , and analogously for the other matrices. For the first set, we have added incoherent noise with $p = 0.1$ (see Eq. (19)) on the states $|\pm x\rangle$, and no additional noise on the remaining states. For the second set, we have added coherent noise with $\epsilon = 0.01$ (see the discussion in the previous subsection) to the state $|-z\rangle$ only. The quantity we have computed for each experiment is

$$\delta_j^* = \frac{1}{4} \sum_{k=1}^4 \delta_{j,k}^*, \quad j = \pm x, \pm y, \pm z, \quad (21)$$

where k labels the effects of the SIC-POVM in Eq. (12) and $\delta_{j,k}^*$ is the output of (11). The results are shown in

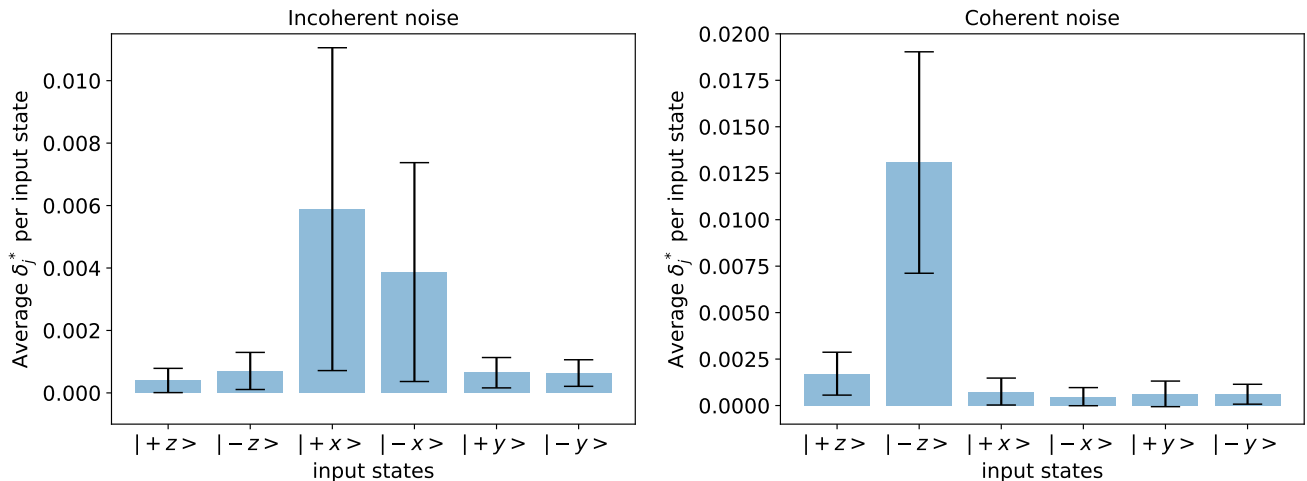


FIG. 5. Average δ_j^* from Eq. (21) per input state over 100 numerical experiments on QMT for the SIC-POVM. The input states are the eigenstates of the Pauli matrices. The error bars are given by the standard deviations of the samples over the different experiments. We are using a total number of shots $n_S = 6 \times 10^5$. Left: incoherent noise with $p = 0.1$ on the states $|\pm x\rangle$. Right: coherent noise with $\epsilon = 0.01$ on the state $|-z\rangle$.

Fig. 5.

We observe that the quantity δ_j^* in Eq. (21), which can be obtained through the many-deltas SDP, signals which input state preparation is noisier, both for coherent and incoherent error. Therefore, this SDP can be employed as a diagnostic tool to recognize which state preparation is making QMT less reliable.

VI. SEE-SAW METHOD FOR SELF-CONSISTENT TOMOGRAPHY

In Sec. VB we have discussed how the SDPs are affected by mismatches between the assumed states and the real ones. As we have seen, we can still have a decent estimation if the level of noise is low. However, if the real states are too far from the assumed ones, our estimation is meaningless.

If we cannot assume to know the set of input states $\{\rho_j\}_{j=1}^N$, we may try to estimate both $\{\rho_j\}_{j=1}^N$ and the set of effects $\{\Pi_k\}_{k=1}^m$ at once, starting from the only data we have access to, that is, the matrix of experimental frequencies f_{jk} . Having a quick look at such a problem, which can still be expressed as in Eq. (7) (where now both ρ_j and Π_k in the vector \mathbf{q} are variables of the optimization problem), however, we realize that this problem is non-linear and non-convex and there is no simple way to solve it. To cope with this issue, many different solutions have been proposed in the literature. These include small gate errors to linearize the problem for gate-set-tomography [18], assuming that states and measurements are globally completable to rewrite the problem as a SDP [20], assuming that there is a subset of known input states [23], using self-testing techniques [49] to perform self-consistent tomography in a photonic setup [24], assuming that there

is a set of noiseless unitary gates that we can apply on the input states [25], or relying on randomized compiling [50] and assumptions on the gates we can apply during the tomographic procedure [26].

In this section, we propose to perform self-consistent measurement tomography, that is, without any assumptions on the set of input states, through a *see-saw* approach to the problem expressed in Eq. (7). In particular, we will focus on the single-delta SDP.

In the see-saw method, we seek to estimate both the measurement and the set of states that were used to obtain the observed frequencies. Thus, we need to use not only an informationally complete set of states, but also an informationally complete (IC) POVM. [46, 51]. Similarly to IC-states, IC-POVMs are defined as POVMs whose effects form a (Hermitian) basis in the space of bounded operators on the system Hilbert space $\mathcal{B}(\mathcal{H})$. Therefore, if the Hilbert space \mathcal{H} has dimension d , a POVM must have at least d^2 linearly independent effects to be informationally complete. These POVMs can be employed to acquire the most general information about the state of the system, since they can be used to reconstruct the density matrix of the quantum system via quantum state tomography (QST) [1].

The see-saw method can be described as follows. Experimentally, we will first perform standard QMT of the POVM we aim to characterize with a chosen set of input states $\{\rho_j^{(0)}\}_{j=1}^N$. This set can be chosen arbitrary, or could be the best guess about the real states. The experimental frequency matrix f_{jk} and the set $\{\rho_j^{(0)}\}_{j=1}^N$ will be the input parameters of the SDP problem in Eq. (8), as usual. The output of the SDP will be a set of effects, say $\{\Pi_k^{(0)}\}_{k=1}^m$, and the value of $\delta^{(0)}$ according to Eq. (9). Due to noise in the input state preparation (and, additionally, to shot noise), $\delta^{(0)}$ will be different from zero,

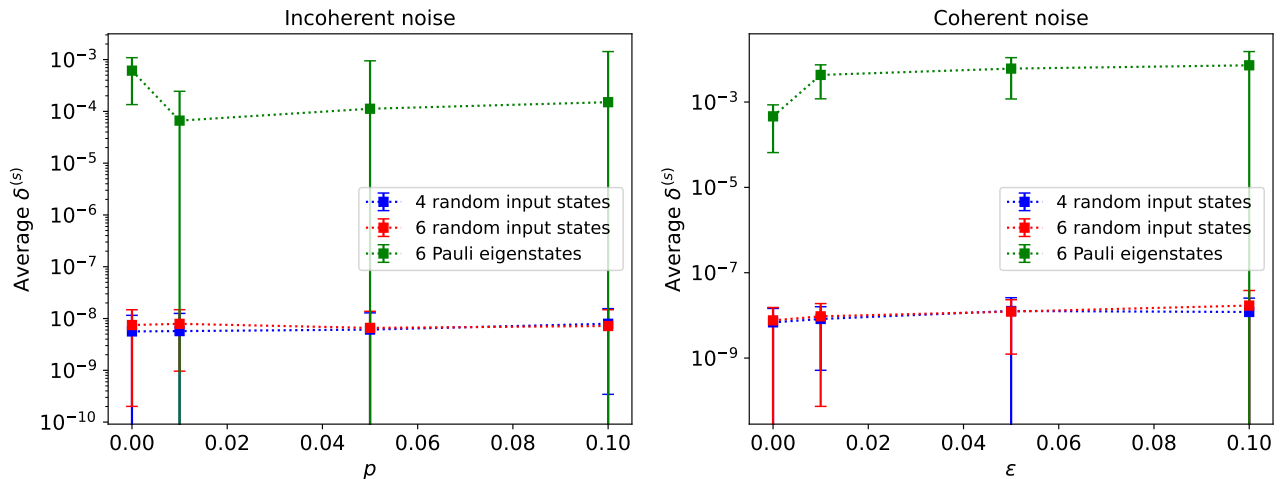


FIG. 6. Average $\delta^{(s)}$ at the final s th step of see-saw according to Eq. (23) with $\nu_\delta = 10^{-7}$, as a function of the noise strength on the input states, for 100 QMT experiments on the SIC-POVM, and with different sets of input states. The error bars are given by the standard deviations of the samples over the different experiments. We are using a total number of shots $n_S = 6 \times 10^5$. Left: incoherent noise. Right: coherent noise.

as discussed in Sec. V. Then, we will run another SDP whose input parameters are the frequency matrix f_{jk} and the set of output effects $\{\Pi_k^{(0)}\}_{k=1}^m$, while the output variables will be a new set of states $\{\rho_j^{(1)}\}_{j=1}^N$ and a new $\delta^{(1)}$. That is, we will perform quantum *state tomography* for the whole set of input states, using as “known” measurement device the POVM returned by the first SDP. The new SDP for QST of the set of input states can be written as:

$$\begin{aligned}
 \min_{\{\rho_j^{(1)}\}} \quad & \delta^{(1)} \\
 \text{s.t.} \quad & f_{jk} - \delta^{(1)} \leq \text{Tr}(\rho_j^{(1)} \Pi_k^{(0)}) \leq f_{jk} + \delta^{(1)} \quad \forall j, k \\
 & \rho_j^{(1)} \geq 0 \quad \forall j \\
 & \text{Tr}[\rho_j^{(1)}] = 1.
 \end{aligned} \tag{22}$$

Clearly, $\delta^{(1)} \leq \delta^{(0)}$. We can therefore repeat this procedure many times, alternating the SDP for QMT and the SDP for QST. Since the overall optimisation problem is not convex, there is no guarantee that this see-saw method will converge towards the optimum. However, we have tested see-saw numerically and observed that, in many scenarios, we can obtain very low values of δ . If after the l^{th} iteration we find $\delta^{(l)} \approx 0$, then we know that $\{\rho^{l-1}\}_{j=1}^N$ and $\{\Pi_k^{(l)}\}_{k=1}^m$ (assuming that the last iteration was a QMT test) consist of pairs of states and effects that are compatible with the measurement statistics. More in particular, the criterion we adopt to stop the see-saw procedure is: interrupt see-saw after the s th step if

$$\delta^{(s)} - \delta^{(s-1)} < \nu_\delta, \tag{23}$$

where ν_δ is a small number we suitably choose. Then, after the s th step, we will have a set of input states

and POVM effects that will match the experimental frequency matrix f_{jk} up to the precision given by $\delta^{(s)}$.

We must stress however that this pair is not unique. There is in general a *gauge transformation* [52] that can be applied to the states and the effects and preserves their mathematical (and physical) properties and conserves the probabilities $\text{Tr}[\rho_j^{(l-1)} \Pi_k^{(l)}]$. This gauge freedom is a well-known issue of self-consistent tomography and gate set tomography, and different optimisation methods have been devised to choose the best gauge [52].

To test see-saw, we have run it in 100 different experiments for the same noisy scenarios we have analyzed in Sec. VB and in Figs. 3 and 4. The results of the average $\delta^{(s)}$ at the final step, with $\nu_\delta = 10^{-7}$ (clearly, the lower ν_δ the most accurate is see-saw, and the longer it takes to run), are depicted in Fig. 6. We note that, for randomly generated states, see-saw with this value of ν_δ converges to very low values of $\delta^{(s)}$, around 10^{-8} , both for coherent and incoherent noise. In contrast, for the very specific set of six eigenstates of the Pauli matrices, see-saw does not always converge to such low values. More insights into see-saw for the Pauli eigenstates are given by Fig. 7, which displays the distribution of $\delta^{(s)}$ for both coherent and incoherent noise. We observe that, despite the average $\delta^{(s)}$ is not very low, see-saw is often decreasing the value of δ^* from Eq. (9) of several orders of magnitude.

VII. CONCLUSIONS

In this work, we have put forward two semidefinite programs (SDPs) for fitting the experimental data of quantum measurement tomography (QMT). The SDPs have been introduced in Sec. IV, where we have also

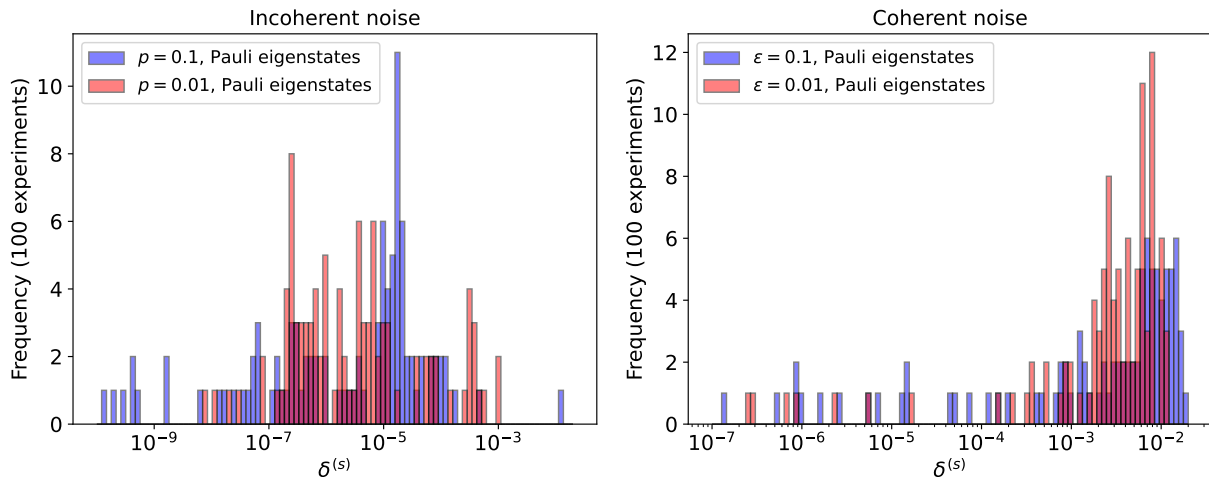


FIG. 7. Distribution of $\delta^{(s)}$ at the final s th step of see-saw according to Eq. (23) with $\nu_\delta = 10^{-7}$, for 100 QMT experiments on the SIC-POVM, and for two different noise strengths. The set of input states consists of the six eigenstates of the Pauli matrices. We are using a total number of shots $n_S = 6 \times 10^5$. Left: incoherent noise. Right: coherent noise.

pointed out that they correspond to minimising the distance between experimental probabilities and ideal quantum probabilities with respect to different norms. The runtime performances of these methods are comparable with the one of the standard log-maximum likelihood estimation, as shown in Appendix A.

In Sec. V we have discussed how the SDPs can be applied to detect noise in real experiments on QMT. We have discussed both shot noise, that is, statistical noise due to a finite number of measurement realizations, and noise in the preparation of the set of input states for QMT. We have shown that the SDPs well-capture the magnitude of shot noise, as well as of coherent noise and incoherent noise on the input states. Moreover, a particular type of SDP, namely the *Many-deltas* SDP corresponding to 1-norm minimisation, can be employed to detect unbalanced noise among the input states.

Finally, in Sec. VI we have discussed how the SDPs for measurement tomography of an informationally-complete POVM may be employed for self-consistent tomography through a *see-saw* optimisation method. The method consists in alternating between a SDP for measurement tomography and state tomography of the whole set of input states. The measurement tomography starts from the experimental frequencies and a set of input states that is typically our best guess about the “real” experimental states and at each step of the see-saw the input parameters are updated according to the output estimates returned by the previous SDP. We have shown that such approach can reach very low values of the parameter $\delta^{(s)}$ that characterizes the mismatch between experimental frequencies and ideal quantum probabilities, thus yielding a set of input states and effects that are compatible with the measurement statistics.

In conclusion, in this work we have shown that SDPs can be a useful, valid and feasible alternative to log-

maximum likelihood estimation in quantum measurement tomography. The insights they give on the errors in QMT make them particularly suitable for the noise analysis of near-term quantum computers. Moreover, the see-saw method is a practical and fast way to perform self-consistent tomography on this type of quantum devices.

ACKNOWLEDGMENTS

We would like to thank Ivano Tavernelli, Francesco Tacchino and Laurin Fischer for interesting discussions on noise detection on quantum hardware. We would also like to thank Carmen Vaccaro for preliminary studies on the runtime of the single-delta SDP, discussed in Appendix A. The SDPs presented in this work are integrated in *Aurora*, a proprietary quantum chemistry platform developed by Algorithmiq Ltd.

Appendix A: Runtime and average accuracy of SDPs for QMT

It is important to compare the performance of the SDPs we have introduced in Sec. IV with the one of the fitting method for QMT that is widely employed in the literature, that is, the log-maximum likelihood estimation (log MLE) [15] whose likelihood functional is given by Eq. (5). In particular, we need to guarantee that the SDPs are not much slower or much less precise than log MLE. To do so, we have performed 100 different QMT numerical experiments with a randomly generated POVM and a set of random linearly independent input states for different dimensions d of the Hilbert space. We have compared the runtime τ that the single-delta and

many-delta SDPs and the log MLE take to process the experimental frequencies, and we have computed the average trace distance between the effects returned by each method and the input effects we employed to sample the probability distribution of each numerical experiment. We have performed these experiments in the case with 10^4 and 5×10^6 shots per input state, and for both complete ($N = d^2$) and overcomplete ($N = d(d + 1)$) sets of input states. The runtimes have been estimated using, for both the SDPs and log MLE, a code written using the CVXPY library for Python [44, 45] with the MOSEK solver [43] and with the same computational power.

The results of the numerical experiments are shown

in Fig. 8 (runtime) and Fig. 9 (average trace distance between input and output effects). We observe that the performances of both the single-delta and the many-deltas SDP are comparable with the ones of log MLE, both as for runtime and for average accuracy. Therefore, we can conclude that these methods are a valid alternative for the fitting of the experimental frequencies in QMT. We note that the runtime of the SDPs as a function of d is sub-exponential [28], and can be captured by a high-degree polynomial. In particular, we have observed that the lines in Fig. 8 are well-reproduced (up to errors of the order of 10^{-12}) by a 5-degree polynomial.

-
- [1] M. A. Nielsen and I. L. Chuang, *Quantum Computation and Quantum Information: 10th Anniversary Edition* (Cambridge University Press, 2010).
- [2] F. B. Maciejewski, Z. Zimborás, and M. Oszmaniec, Mitigation of readout noise in near-term quantum devices by classical post-processing based on detector tomography, *Quantum* **4**, 10.22331/q-2020-04-24-257 (2020).
- [3] Y. Chen, M. Farahzad, S. Yoo, and T.-C. Wei, Detector tomography on ibm quantum computers and mitigation of an imperfect measurement, *Physical Review A* **100**, 052315 (2019).
- [4] M. R. Geller, Rigorous measurement error correction, *Quantum Science and Technology* **5**, 03LT01 (2020).
- [5] F. B. Maciejewski, F. Baccari, Z. Zimborás, and M. Oszmaniec, Modeling and mitigation of cross-talk effects in readout noise with applications to the quantum approximate optimization algorithm, *Quantum* **5**, 464 (2021).
- [6] S. Bravyi, S. Sheldon, A. Kandala, D. C. McKay, and J. M. Gambetta, Mitigating measurement errors in multiqubit experiments, *Physical Review A* **103**, 042605 (2021).
- [7] P. D. Nation, H. Kang, N. Sundaresan, and J. M. Gambetta, Scalable mitigation of measurement errors on quantum computers, *PRX Quantum* **2**, 040326 (2021).
- [8] M. L. Dahlhauser and T. S. Humble, Modeling noisy quantum circuits using experimental characterization, *Physical Review A* **103**, 042603 (2021).
- [9] L. Funcke, T. Hartung, K. Jansen, S. Kühn, P. Stornati, and X. Wang, Measurement error mitigation in quantum computers through classical bit-flip correction, *Physical Review A* **105**, 062404 (2022).
- [10] G. García-Pérez, M. A. Rossi, B. Sokolov, F. Tacchino, P. K. Barkoutsos, G. Mazzola, I. Tavernelli, and S. Maniscalco, Learning to measure: Adaptive informationally complete generalized measurements for quantum algorithms, *PRX Quantum* **2**, 10.1103/prxquantum.2.040342 (2021).
- [11] A. Glos, A. Nykänen, E.-M. Borrelli, S. Maniscalco, M. A. C. Rossi, Z. Zimborás, and G. García-Pérez, Adaptive POVM implementations and measurement error mitigation strategies for near-term quantum devices, arXiv:2208.07817 (2022).
- [12] H.-Y. Huang, R. Kueng, and J. Preskill, Predicting many properties of a quantum system from very few measurements, *Nature Physics* **16**, 1050 (2020).
- [13] H.-Y. Huang, R. Kueng, and J. Preskill, Efficient estimation of pauli observables by derandomization, *Physical review letters* **127**, 030503 (2021).
- [14] C. Hadfield, S. Bravyi, R. Raymond, and A. Mezzacapo, Measurements of quantum hamiltonians with locally-biased classical shadows, *Communications in Mathematical Physics* **391**, 951 (2022).
- [15] J. Fiurášek, Maximum-likelihood estimation of quantum measurement, *Physical Review A* **64**, 024102 (2001).
- [16] D. Mogilevtsev, J. Řeháček, and Z. Hradil, Self-calibration for self-consistent tomography, *New Journal of Physics* **14**, 095001 (2012).
- [17] D. Mogilevtsev, A. Ignatenko, A. Maloshtan, B. Stoklasa, J. Rehacek, and Z. Hradil, Data pattern tomography: reconstruction with an unknown apparatus, *New Journal of Physics* **15**, 025038 (2013).
- [18] S. T. Merkel, J. M. Gambetta, J. A. Smolin, S. Poletto, A. D. Córcoles, B. R. Johnson, C. A. Ryan, and M. Steffen, Self-consistent quantum process tomography, *Physical Review A* **87**, 062119 (2013).
- [19] R. Blume-Kohout, J. K. Gamble, E. Nielsen, J. Mizrahi, J. D. Sterk, and P. Maunz, Robust, self-consistent, closed-form tomography of quantum logic gates on a trapped ion qubit, preprint arXiv:1310.4492 (2013).
- [20] C. Stark, Self-consistent tomography of the state-measurement gram matrix, *Physical Review A* **89**, 052109 (2014).
- [21] C. Jackson and S. J. van Enk, Detecting correlated errors in state-preparation-and-measurement tomography, *Physical Review A* **92**, 042312 (2015).
- [22] A. F. McCormick, S. J. V. Enk, and M. Beck, Experimental demonstration of loop state-preparation-and-measurement tomography, *Physical Review A* **95**, 10.1103/PhysRevA.95.042329 (2017).
- [23] A. C. Keith, C. H. Baldwin, S. Glancy, and E. Knill, Joint quantum-state and measurement tomography with incomplete measurements, *Physical Review A* **98**, 10.1103/PhysRevA.98.042318 (2018).
- [24] A. Zhang, J. Xie, H. Xu, K. Zheng, H. Zhang, Y.-T. Poon, V. Vedral, and L. Zhang, Experimental self-characterization of quantum measurements, *Physical Review Letters* **124**, 040402 (2020).
- [25] A. Stephens, J. M. Cutshall, T. McPhee, and M. Beck, Self-consistent state and measurement tomography with fewer measurements, *Physical Review A* **104**,

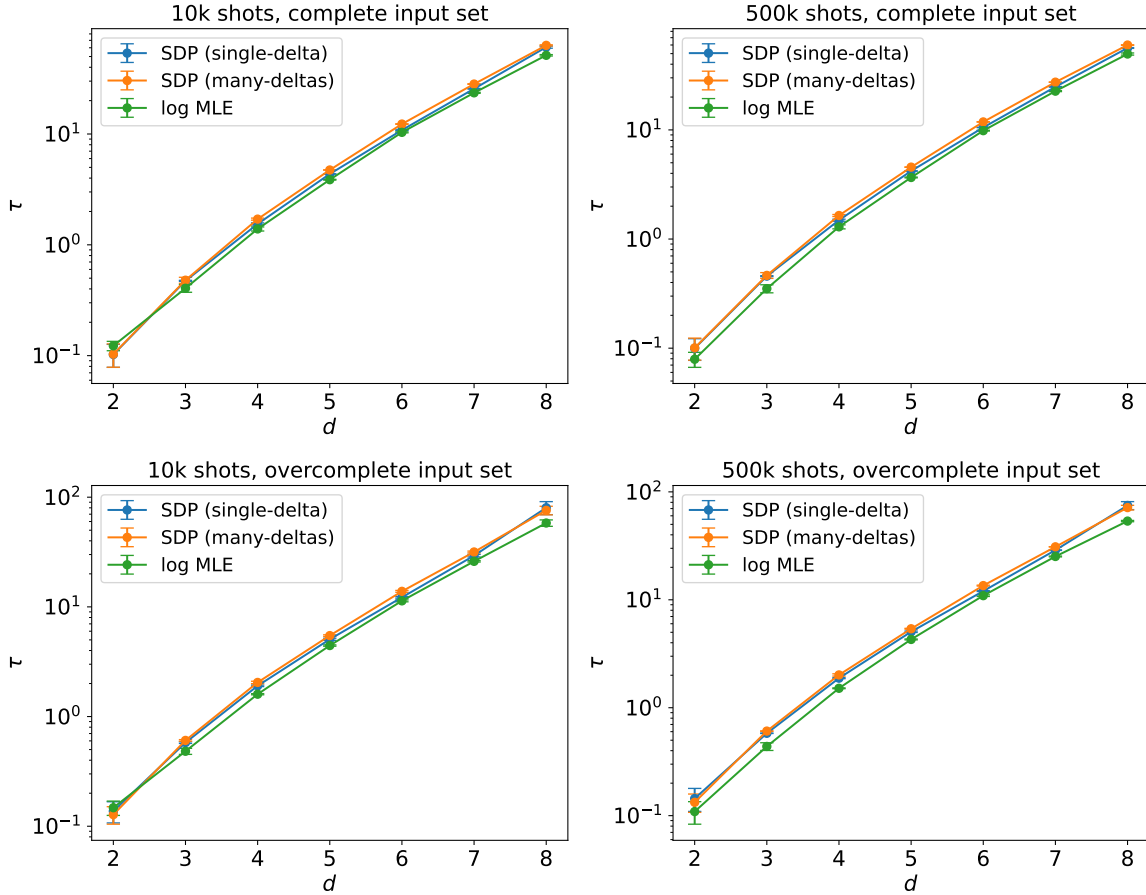


FIG. 8. Runtime τ of single-delta SDP (blue), many-deltas SDP (orange), and log MLE (green) as a function of the dimension d of the Hilbert space of the quantum system. The error bars are the standard deviations of the values over 100 different numerical experiments. We employ either 10^4 or 5×10^6 shots per input state, and a complete ($N = d^2$) or overcomplete ($N = d(d + 1)$) set of random input states.

- 10.1103/PhysRevA.104.012416 (2021).
- [26] J. Lin, J. J. Wallman, I. Hincks, and R. Laflamme, Independent state and measurement characterization for quantum computers, *Physical Review Research* **3**, 10.1103/PhysRevResearch.3.033285 (2021).
- [27] H. Landa, D. Meiroum, N. Kanazawa, M. Fitzpatrick, and C. J. Wood, Experimental bayesian estimation of quantum state preparation, measurement, and gate errors in multiqubit devices, *Physical Review Research* **4**, 10.1103/PhysRevResearch.4.013199 (2022).
- [28] S. Boyd and L. Vandenberghe, *Convex Optimization* (Cambridge University Press, 2004).
- [29] P. Skrzypczyk and D. Cavalcanti, *Semidefinite Programming in Quantum Information Science* (IOP Publishing, 2023).
- [30] H. B. Coldenstrodt-Ronge, J. S. Lundeen, K. L. Pregnell, A. Feito, B. J. Smith, W. Maurer, C. Silberhorn, J. Eisert, M. B. Plenio, and I. A. Walmsley, A proposed testbed for detector tomography, *Journal of Modern Optics* **56**, 432 (2009).
- [31] J. S. Lundeen, A. Feito, H. Coldenstrodt-Ronge, K. L. Pregnell, C. Silberhorn, T. C. Ralph, J. Eisert, M. B. Plenio, and I. A. Walmsley, Tomography of quantum detectors, *Nature Physics* **5**, 27 (2009).
- [32] A. Feito, J. S. Lundeen, H. Coldenstrodt-Ronge, J. Eisert, M. B. Plenio, and I. A. Walmsley, Measuring measurement: Theory and practice, *New Journal of Physics* **11**, 10.1088/1367-2630/11/9/093038 (2009).
- [33] L. Zhang, A. Datta, H. B. Coldenstrodt-Ronge, X. M. Jin, J. Eisert, M. B. Plenio, and I. A. Walmsley, Recursive quantum detector tomography, *New Journal of Physics* **14**, 10.1088/1367-2630/14/11/115005 (2012).
- [34] L. Zhang, H. B. Coldenstrodt-Ronge, A. Datta, G. Puentes, J. S. Lundeen, X. M. Jin, B. J. Smith, M. B. Plenio, and I. A. Walmsley, Mapping coherence in measurement via full quantum tomography of a hybrid optical detector, *Nature Photonics* **6**, 364 (2012).
- [35] A. Luis and L. L. Sánchez-Soto, Complete characterization of arbitrary quantum measurement processes, *Physical Review Letters* **83**, 3573 (1999).
- [36] G. M. D'Ariano, L. Maccone, and P. L. Presti, Quantum calibration of measurement instrumentation, *Physical Review Letters* **93**, 10.1103/PhysRevLett.93.250407 (2004).
- [37] Z. Hradil, J. Řeháček, J. Fiurášek, and M. Ježek, 3 maximum-likelihood methods in quantum mechanics, in *Quantum state estimation* (Springer, 2004) pp. 59–112.
- [38] R. Kosut, I. A. Walmsley, and H. Rabitz, Optimal ex-

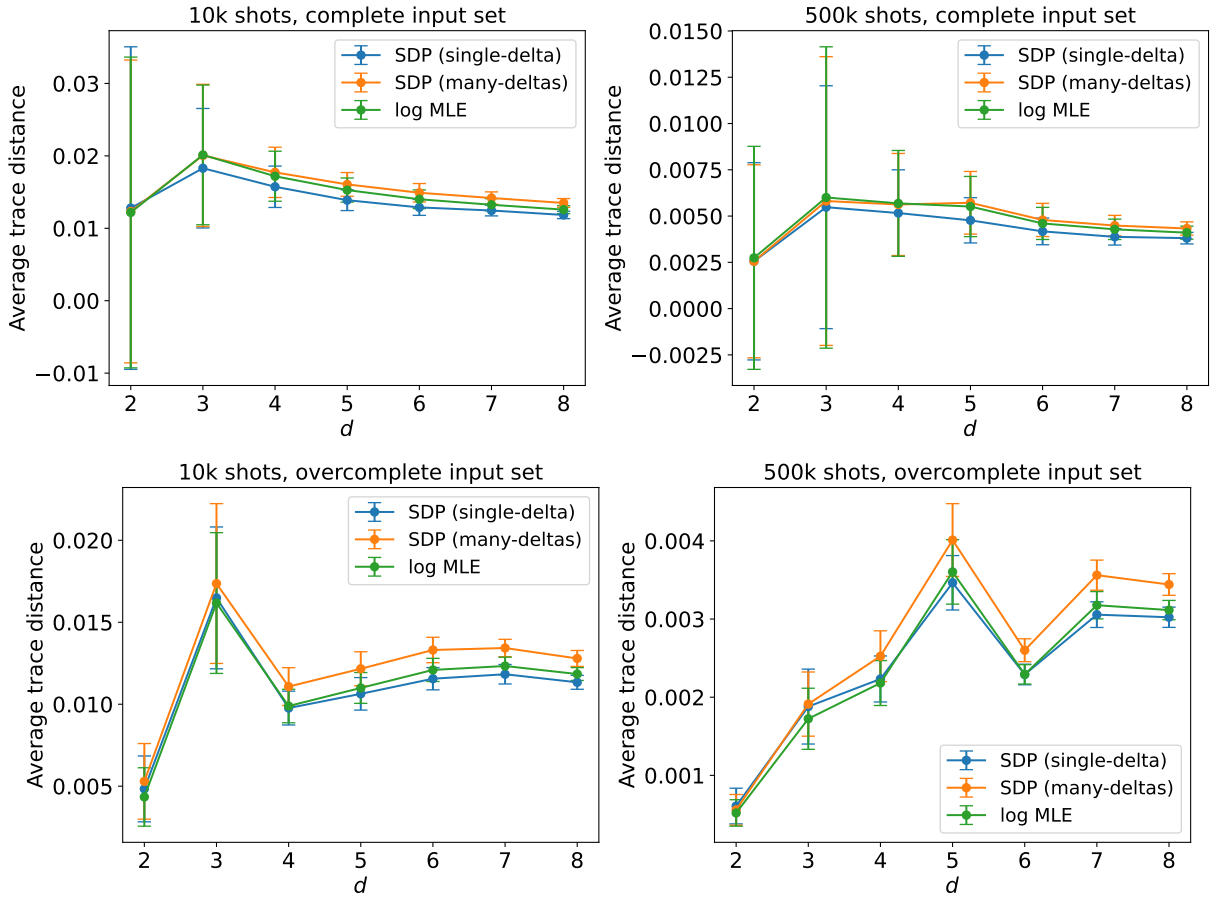


FIG. 9. Average trace distance between the “ideal effects” and the output effects returned by the single-delta SDP (blue), many-deltas SDP (orange), and log MLE (green) as a function of the dimension d of the Hilbert space of the quantum system. The error bars are the standard deviations of the values over 100 different numerical experiments. We employ either 10^4 or 5×10^6 shots per input state, and a complete ($N = d^2$) or overcomplete ($N = d(d + 1)$) set of random input states.

periment design for quantum state and process tomography and hamiltonian parameter estimation, preprint arXiv:quant-ph/0411093 (2004).

- [39] J. A. Smolin, J. M. Gambetta, and G. Smith, Efficient method for computing the maximum-likelihood quantum state from measurements with additive gaussian noise, *Physical Review Letters* **108**, 070502 (2012).
- [40] Y. Wang, S. Yokoyama, D. Dong, I. R. Petersen, E. H. Huntington, and H. Yonezawa, Two-stage estimation for quantum detector tomography: Error analysis, numerical and experimental results, *IEEE Transactions on Information Theory* **67**, 2293 (2021).
- [41] S. Xiao, Y. Wang, D. Dong, and J. Zhang, Optimal quantum detector tomography via linear regression estimation (Institute of Electrical and Electronics Engineers Inc., 2021) pp. 4140–4145.
- [42] S. Xiao, Y. Wang, D. Dong, and J. Zhang, Optimal and two-step adaptive quantum detector tomography, *Automatica* **141**, 10.1016/j.automatica.2022.110296 (2022).
- [43] MOSEK ApS, *MOSEK Optimizer API for Python 10.0.33* (2019).
- [44] S. Diamond and S. Boyd, CVXPY: A Python-embedded modeling language for convex optimization, *Journal of Machine Learning Research* **17**, 1 (2016).
- [45] A. Agrawal, R. Verschueren, S. Diamond, and S. Boyd, A rewriting system for convex optimization problems, *Journal of Control and Decision* **5**, 42 (2018).
- [46] S. T. Flammia, A. Silberfarb, and C. M. Caves, Minimal informationally complete measurements for pure states, *Foundations of Physics* **35**, 1985 (2005).
- [47] J. Johansson, P. Nation, and F. Nori, Qutip: An open-source python framework for the dynamics of open quantum systems, *Computer Physics Communications* **183**, 1760 (2012).
- [48] M. Ozols, How to generate a random unitary matrix (2009).
- [49] A. Tavakoli, J. Kaniewski, T. Vértesi, D. Rosset, and N. Brunner, Self-testing quantum states and measurements in the prepare-and-measure scenario, *Physical Review A* **98**, 062307 (2018).
- [50] J. J. Wallman and J. Emerson, Noise tailoring for scalable quantum computation via randomized compiling, *Physical Review A* **94**, 052325 (2016).
- [51] P. Busch and P. J. Lahti, The determination of the past and the future of a physical system in quantum mechanics, *Foundations of Physics* **19**, 633 (1989).
- [52] E. Nielsen, J. K. Gamble, K. Rudinger, T. Scholten, K. Young, and R. Blume-Kohout, Gate set tomography,

